Apparent Tradeoff of Higher Activity in MMP-12 for Enhanced Stability and Flexibility in MMP-3

Xiangyang Liang, A. Arunima, Yingchu Zhao, Rajagopalan Bhaskaran, Anuradha Shende, Todd S. Byrne, Jeremy Fleeks, Mark O. Palmier, and Steven R. Van Doren*
Department of Biochemistry, University of Missouri, Columbia, Missouri

ABSTRACT The greater activity of MMP-12 than MMP-3 toward substrates from protein fibrils has been quantified. Why is MMP-12 the more active protease? We looked for behaviors associated with the higher activity of MMP-12 than MMP-3, using nuclear magnetic resonance to monitor backbone dynamics and residue-specific stabilities of their catalytic domain. The proteolytic activities are likely to play important roles in inflammatory diseases of arteries, lungs, joints, and intestines. Nuclear magnetic resonance line broadening indicates that regions surrounding the active sites of both proteases sample conformational substates within milliseconds. The more extensive line broadening in MMP-3 suggests greater sampling of conformational substates, affecting the full length of helix B and β-strand IV forming the active site, and more remote sites. This could suggest more excursions to functionally incompetent substates. MMP-3 also has enhanced subnanosecond fluctuations in helix A, in the β-hairpin of strands IV and V, and before and including helix C. Hydrogen exchange protection in the EX2 regime suggests that MMP-3 possesses 2.8 kcal/mol higher folding stability than MMP-12(E219A). The β-sheet of MMP-3 appears to be stabilized still more. The higher stability of MMP-3 relative to MMP-12 coincides with the former's considerably lower proteolytic activity. This relationship is consistent with the hypothesis that enzymes often trade stability for higher activity.

INTRODUCTION

Elucidating relationships of dynamics in enzyme function is an important challenge. Activity of diverse enzymes has been related not only to their intrinsic dynamics on picosecond-to-millisecond timescales as reviewed by Boehr et al. (1), but also to their folding stability (2,3). The stability-function hypothesis suggests that optimization of enzymes to enable interaction with substrates and transition states detracts from internal packing interactions that would stabilize the protein structure, conferring marginal stability (2,3). Herein, we compare the activities, backbone fluctuations, and folding stability of two metallated proteases, as part of an effort to account for differences in their activity that would appear to be significant in the context of inflammatory diseases.

The proteolytic enzyme matrix metalloproteinase-12 (MMP-12 or metalloelastase) secreted by macrophages holds special interest due to its importance in major diseases of arteries and lungs, regulation of inflammatory responses in lungs, and digestion of key protein substrates, including fibrils such as elastin that resist hydrolysis (4).

Biochemical investigations (5) (C. M. Overall, University of British Columbia, personal communication, 2008) have raised the question: Why is MMP-12 so active? Because MMP-12 undergoes rapid autolysis (self-degradation), neither the physiological nor the purified active form of MMP-12 retains the C-terminal domain (4). The degradation of elastin by MMP-12 in chronic inflammatory diseases of the lungs and arteries is significant because the heavily cross-linked elastin fibrils provide the elastic recoil of lungs and arteries, and release of elastin fragments amplifies and prolongs the inflammatory response in emphysema (6,7). MMP-12 activity appears to exacerbate atherosclerosis (8) and abdominal aortic aneurysms (9). Collagen V (from ubiquitous collagen I fibrils) and a triple helical peptide derived from it also resist proteolysis, except by MMP-2, -9, and -12 (10–12). Alpha1-antitrypsin, collagen IV, and several other components of the extracellular matrix are also readily hydrolyzed by MMP-12 (13). MMP-12 readily truncates a class of CXC chemokines, rendering them unable to bind their receptors and providing macrophages a way to regulate acute inflammation and resolve the initial phase of acute inflammation of infected lungs (5).

MMP-3 (stromelysin 1) shares 60% sequence identity with MMP-12 in the catalytic domain, making them closest homologs. MMP-3 is associated with the cartilage degradation and inflammation of rheumatoid arthritis and osteoarthritis (14). Soon after stroke, MMP-3 opens the blood-brain barrier by attacking tight junctions and basal lamina (15).

Why MMP-12 is so active among MMPs is not clear in the structural coordinates. The backbone conformation of the catalytic domain of MMP-12 scarcely differs from that of other MMPs (16). The active site clefts of the MMPs are mostly conserved, with the exception of the S1′ specificity loops. MMPs 12, 3, 8, and 13 form a group with the largest S1′ specificity pockets (17). Despite the high structural

Submitted December 17, 2009, and accepted for publication April 1, 2010.

*Correspondence: vandorens@missouri.edu

Xiangyang Liang's present address is R&D Systems Inc., Minneapolis, MN.

Rajagopalan Bhaskaran's present address is Department of Chemistry and Biochemistry, Auburn University, Auburn, AL.

Anuradha Shende's present address is Chemical and Biological Engineering Department, South Dakota School of Mines and Technology, Rapid City, SD.

Editor: Patrick Loria.

0006-3495/10/07/0273/11 $2.00

doi: 10.1016/j.bpj.2010.04.002

similarities among MMP catalytic domain, MMP-12 possesses the only catalytic domain known to be sufficient for high activity toward protease-resistant elastin (4), collagen V (11), a triple helical peptide from collagen V (12), and the ELR sequence of CXC chemokines (5). In contrast, MMP-2 and -9 require their fibronectin-like inserts for elastolytic (18) and collagenolytic activities (19,20).

We have investigated whether dynamics and stability could be factors in the high activities of MMP-12 toward pathophysiologically important substrates. In inhibitor complexes of MMPs, loops of the catalytic domain display a structural variability suggesting mobility (16,21) that is partially corroborated by nuclear magnetic resonance (NMR) relaxation of the loops (21,22). Backbone dynamics studies of inhibitor complexes of MMP-3 catalytic domain found the S1–S3 subsites to be rigid and the S1′-S3′ subsites to be rigid with inhibitor bound to them but flexible when inhibitors instead occupied the S1–S3 subsites (23). We have quantitatively compared the activity, backbone rigidity, and stability (under EX2 conditions) of the catalytic domain of MMP-12 and MMP-3, both unfettered by inhibitor. The catalytic domain of MMP-12 exhibits clearly higher activity, more rigidity of its backbone, and lower folding stability than its counterpart of the MMP-3 catalytic domain that has more internal motions throughout. The greater stability of less active MMP-3 catalytic domain is consistent with the hypothesis of tradeoffs between stability and function, whereby stabilizing mutations of enzymes diminish activity (2).

MATERIALS AND METHODS

^{15}N NMR relaxation and its interpretation

The ^{15}N relaxation rates of TROSY-sharpened $R_2{}^{\alpha}$, fast relaxing $R_2{}^{\beta}$, and two-spin order $R_1{}^{2HzNz}$ were measured at 81.1 MHz using pulse sequences and relaxation periods incremented in time steps of $(\pi J_{NH})^{-1}$ (24). The cross-correlation rate η_{xy} was determined from $R_2{}^{\alpha}$ and $R_2{}^{\beta}$ (24) and directly using the pulse sequence of Liu and Prestegard (25) with a constant time period of 42 ms. The exchange broadening R_{ex} results from this combination of the relaxation rates,

$$R_{ex} = R_2^{\alpha} - R_1^{2HzNz}/2 - \eta_{xy}(\kappa - 1) + R_1^{N}/2, \qquad (1)$$

where κ is 1.4 from the trimmed mean of $1 + (R_2{}^{\alpha}\text{-}R_1{}^{2HzNz}/2)/\eta_{xy}$ (24). The baseline scatter (Fig. 1, *c* and *d*) was attributed to variability in the ^{15}N CSA tensors (24).

^{15}N relaxation rates R_1 and R_2 were measured with pulse sequences (26) enhanced with flip back pulses. The CPMG trains for R_2 employed radio-frequency field strength γB_1 of 7200 Hz with π-pulses spaced 1.2 ms apart. Relaxation periods for R_1 ranged from 20 to 600 ms at 60.8 MHz or to 800 ms at 50.7 MHz and from 10 to 130 ms for R_2 at 60.8 MHz. Fitting uncertainties in relaxation rates were simulated by introducing random error with SPARKY. Five pairs of $\{^1H\}^{15}N$ steady-state nuclear Overhauser effect (NOE) spectra of MMP-12 (E219A) and six pairs for MMP-3 catalytic domain provided averages and standard deviations. Steady-state $^{15}N\{^1H\}$ NOE spectra (26) were measured with and without 4 s of proton saturation, in an interleaved manner to maintain identical conditions. The unsaturated reference spectra used relaxation delays of 6 s to allow water magnetization to recover. A TROSY-enhanced, relaxation-compensated CPMG pulse sequence was used to identify sites of chemical exchange broadening (27). Its π-pulses were issued with γB_1 of 5100 Hz. Delays used within the CPMG trains were $\tau_{cp} = 0.833$ ms or 5.5 ms, i.e., 1.7 ms or 11 ms between π pulses. Relaxation periods for the exponential decays ranged up to 154 ms. Uniformity of recovery was improved with the DCCPSS- pre-sequence (28).

To identify residues that were free of internal motion and with the ^{15}N relaxation suitable for modeling rotational correlation time τ_c and diffusion tensor, coarse-filtering was performed to remove mobile residues evident by low $\{^1H\}^{15}N$ NOE or high ^{15}N R_2 (unless ^{15}N R_1 is low) (29). Fine filtering followed, according to Ding et al. (30). Diffusion tensor parameters θ, ϕ, $D_{\parallel}$, and $D_{\perp}$ were fitted to the fine-filtered set of residues, their 60.8-MHz R_1 and R_2 values, using Tensor2 (31), and PDB coordinates 1bm6 for MMP-3 catalytic domain and 2poj for MMP-12(E219A). Model-free simulations fitted the relaxation measurements at 60.8 MHz (R_1, R_2, and $^{15}N\{^1H\}$ NOE) and 50.7 MHz (R_1) to one of five spectral density functions (Table S3 in the Supporting Material) using the program ModelFree 4.1 by Professor A. G. Palmer. The ^{15}N CSA was set to the approximation of -170 ppm and the N-H bond length to 1.02 Å. Akaike's information criterion was used for statistical selection of spectral density functions differing in use of τ_e and R_{ex} (32).

Hydrogen exchange protection

Hydrogen-deuterium exchange (HDX) was initiated by dissolving the lyophilized MMP in ^2H_2O and centrifuging briefly to remove undissolved protein. HDX rates in MMP-12(E219A) and MMP-3 catalytic domain were monitored by a series of ^{15}N HSQC spectra at 26°C and 600 MHz collected over periods of 72 and 86 h, respectively. Each exchange rate k_{ex} is the exponential decay rate constant fitted to the decay of peak heights with time after dissolving in ^2H_2O. The intrinsic rate of random coil HX, k_{rc}, was calculated (33) using the program SPHERE (http://www.fccc.edu/research/labs/roder/sphere/sphere.html). The Gibbs free energy of protection from hydrogen exchange, ΔG_{HX}, was calculated from k_{ex} and k_{rc} (adjusted for the conditions of pH 6.6 and 26°C) using Eq. 2 (33):

$$\Delta G_{HX} = -RT\ln(k_{ex}/k_{rc}). \qquad (2)$$

RESULTS

MMP-12 is more active than MMP-3

We compared proteolytic enzyme kinetics, backbone dynamics, and stabilities of the inhibitor-free catalytic domain of MMP-3 and MMP-12. We refer to the former as MMP-3 catalytic domain. NMR studies used MMP-12 preserved by E219A substitution of the general base (12,34), which we name MMP-12(E219A), inasmuch as its active form in vivo retains only the catalytic domain (4). MMP-12 exhibits higher, and MMP-3 catalytic domain lower, second-order rate constants, k_{cat}/K_m, toward a short peptide substrate (FS-6), substrates from protease-resistant elastin and collagen V fibrils (fELN-125 and α1(V) THP), and substrates from collagen I and IV, as listed in Table 1. The differing activities but close structural resemblance and 60% sequence identity of these two MMP catalytic domain makes them well suited for comparing properties that would distinguish them.

Millisecond fluctuations surround active site, especially in MMP-3

We investigated the scope of conformational fluctuations occurring in the backbone of each protease within

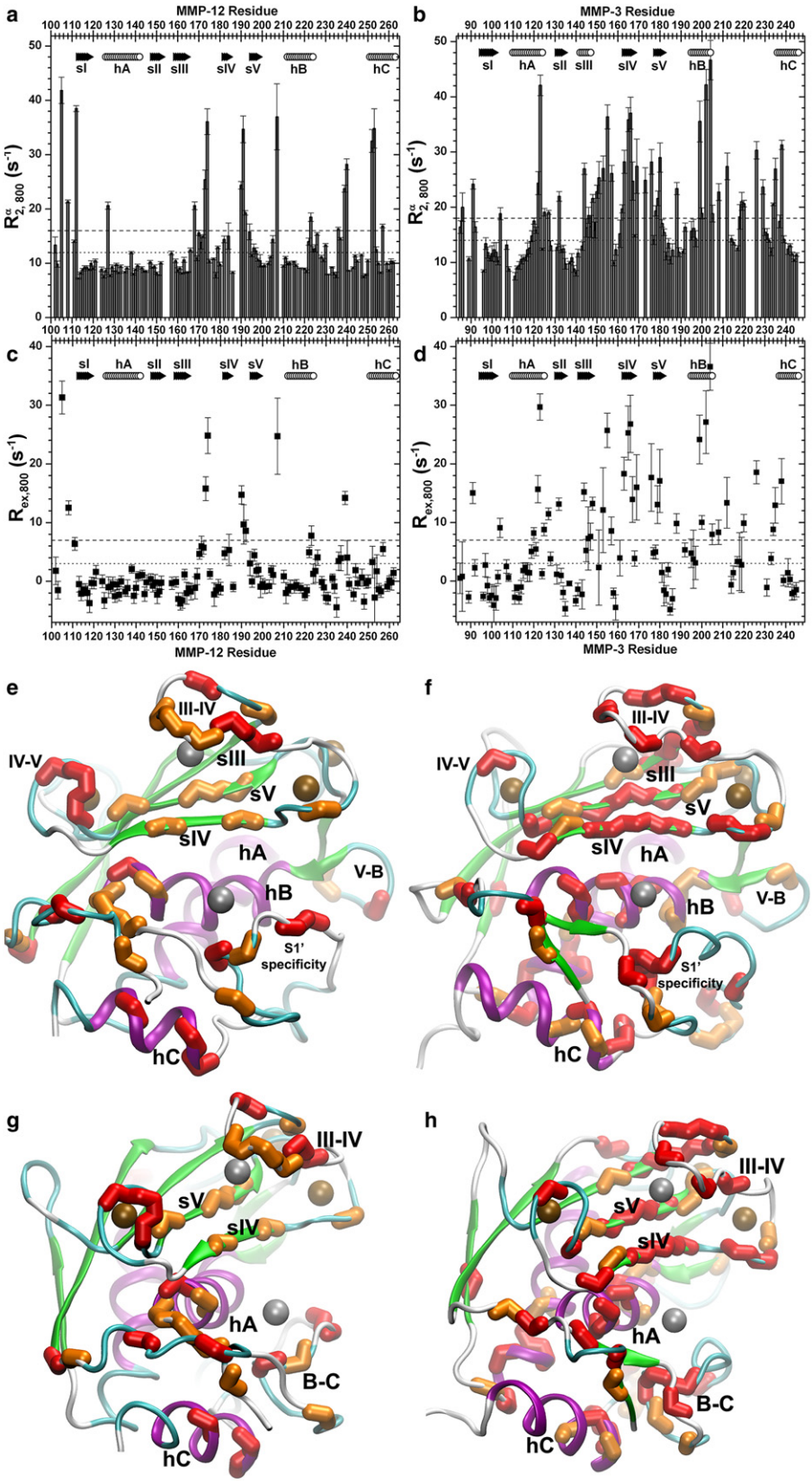

FIGURE 1 Sites of conformational exchange within milliseconds in MMP-12(E219A) (*left panels*) and MMP-3 catalytic domain (*right panels*) are identified by high $R_2{}^{\alpha}$ Hahn spin echo relaxation rates at 81 MHz (*a* and *b*) and high R_{ex} exchange broadening (*c* and *d*). Secondary structure is marked by arrows for β-strands and cylinders for α-helices. (*e–h*) Residues with red (*darker gray*) backbone atoms have $R_2{}^{\alpha}$ or R_{ex} at least 7 s^{-1} greater than (*upper threshold*) the trimmed mean of unaffected residues. In panels *e–h*, orange (*lighter gray*) residues have $R_2{}^{\alpha}$ or R_{ex} at least 3 s^{-1} greater (*lower threshold lines*). (*e* and *f*) Standard orientation with active site cleft running horizontally. (*g* and *h*) View from the side, placing the cleft at right. Zinc ions are in gray and calcium ions are in bronze (*darker gray*). Helices are colored purple (*darker gray*) and β-strands green (*lighter gray*) in the inhibitor free structures of MMP-12(E219A) in solution (33) (*e*, PDB entry 2poj) and MMP-3 catalytic domain in crystals (57) (*f*, PDB entry 1cqr).

TABLE 1 Kinetics of human MMP-12 and -3 catalytic domain at 25°C

	General metalloprotease substrate FS-6	Elastin fELN-125	DQ-col I	DQ-col IV	Triple helical peptide α1(V) fTHP[†]
Catalytic domain	k_{cat}/K_m, M^{-1} s^{-1}	k_{cat}/K_m, M^{-1} s^{-1}	k_{cat}/K_m, M^{-1} s^{-1}	k_{cat}/K_m, M^{-1} s^{-1}	k_{cat}/K_m, M^{-1} s^{-1}
MMP-12	**133,800 ± 650**	**9880 ± 480**	**34,600 ± 700**	**29,200 ± 200**	**55,400 ± 100**[‡]
MMP-3	20,630 ± 30	830 ± 10	14,040 ± 30	110 ± 10	<48[§]
$\frac{MMP-12}{MMP-3}$	6.5-fold	12-fold	2.5-fold	265-fold	>1000-fold

Derived from individual progress curves at low substrate in 0.1 M Tris-HCl (pH 7.5), 0.1 M NaCl, 10 mM NaCl, and 0.1 mM $ZnCl_2$, as described in the literature (12,43,56). Bold indicates an advantage in catalytic turnover rate k_{cat} according to M. O. Palmier, Y. G. Fulcher, and S. R. Van Doren (unpublished). Note that "f" means "labeled with fluorescent BODIPY for FRET assay", and "125" means "full-length, with apparent molecular mass of 125 kDa by SDS-PAGE".

[†]Mimics the MMP cleavage site within residues 436–447 of the α1 chain of collagen V (43).

[‡]From Bhaskaran et al. (12).

[§]From Lauer-Fields et al. (10).

milliseconds, evident as exchange broadening of ^{15}N NMR lines resulting from equilibria with alternate structural or chemical environments. We used dilute monodisperse solutions of 0.15 mM MMP-3 catalytic domain and 0.21 mM MMP-12(E219A) to avoid effects of self-association, as described in the Supporting Material. ^{15}N NMR line broadening from dynamic equilibria was maximized using both the high magnetic field strength of 800 MHz equipment and a Hahn spin echo with only one π-pulse (24). The method relies upon measuring the transverse relaxation rate $R_2{}^{\alpha}$ from the narrow member of the ^{15}N doublet. The inherently slow TROSY relaxation of $R_2{}^{\alpha}$ provides much dynamic range for monitoring the exchange broadening R_{ex}. Contributions from relaxation rates called longitudinal two-spin order $R_1{}^{2HzNz}$, cross-correlation rate η_{xy}, and $R_1{}^{N}$ were subtracted from $R_2{}^{\alpha}$ to estimate R_{ex} (Eq. 1) (24). In both MMP-12(E219A) and MMP-3 catalytic domain, elevation of ^{15}N $R_2{}^{\alpha}$ and R_{ex} is observed in seven locales: the N-terminus; the S-shaped III–IV loop; the β-hairpin formed by strands IV and V (sIV–sV); the V-B loop; the C-terminal end of helix B (hB); the B-C loop residues that include the lower lip of the active site cleft; and the N-terminal half of helix C (hC) (Fig. 1). These comprise 37 residues of MMP-12(E219A) and at least 63 residues of MMP-3 catalytic domain. These regions with excess line broadening from conformational fluctuations surround the active site cleft. The enrichment of peaks of MMP-3 catalytic domain with severe line broadening (Fig. 1) is striking throughout hB and sIV that form the active site cleft, in adjacent β-strand sV, near the C-terminal end of sIII, and at the C-terminal end of hA that abuts hB on the back (Fig. 1, *f* and *h*). The excess line broadening implies that the regions around the active sites undergo fluctuations within milliseconds to conformational substates of modestly higher free energy, especially throughout hB and sIV of the MMP-3 active site. The envelopment of the active site by regions with millisecond motions is clarified in the side views of Fig. 1, *g* and *h*.

Almost half or 17 of the same residues of MMP-12(E219A), plus seven others, also exhibit less line broadening in relaxation dispersion at 61 MHz (Fig. 2 *a*). The timescales of these conformational fluctuations overlap the range between the 1.7 ms and 11 ms delay periods between the π-pulses of the TROSY-CPMG pulse sequence (27).These 24 residues cluster on the left side, at C-terminal ends of sIV and hB at the active site, and in loops near the active site in the N-terminus, III–IV, IV–V, V-B, and B-C (S1′ specificity) loops (Fig. 2 *e*). The distal II–III loop is also affected. A smaller subset of 11 residues already identified in MMP-12(E219A) also exhibit line broadening from conformational fluctuations occurring within the 1.2 ms CPMG delay periods of conventional ^{15}N R_2 relaxation at 61 MHz (Fig. 2 *c*). This rate of pulsing may suppress most line broadening present during much longer spacing used in measuring $R_2{}^{\alpha}$ (Fig. 1 *a*). The broadening remaining with the faster pulsing suggest the exchange processes to be faster at these positions, e.g., in sIV and adjoining loops (Fig. 2 *c*), than elsewhere. The relaxation data from 800- and 600-MHz systems together identify exchange broadening in 46 residues of MMP-12(E219A).

In MMP-3 catalytic domain, elevated ^{15}N R_2 values or relaxation dispersion at 61 MHz confirmed line broadening in 25 residues and revealed 21 additional residues with line broadening not quantifiable in the 81-MHz relaxation data (Fig. 2, *b* and *d*). Nearly all in this latter group sequentially neighbor amide groups with exchange broadening in the 81-MHz relaxation data (Fig. 2 *f*). The lesser exchange broadening in the measurements at 61 MHz both missed many cases evident at 81 MHz and detected many cases of exchange broadening too extreme to describe from the 81-MHz relaxation data. The broadening remaining with 1.2-ms spacing of π-pulses suggests faster exchange rates in four loops (Fig. 2 *d*) than elsewhere. The amide groups with 2 s^{-1} or more of exchange broadening in the ^{15}N R_2 values or relaxation dispersion at 61 MHz are found around the active site at sIV (His-166 coordinating the structural zinc), IV-V loop, V-B loop, hB, and the B-C or S1′ specificity loop of MMP-3 catalytic domain. The exchange broadening also maps to the N-terminus, N-terminal end of hA,

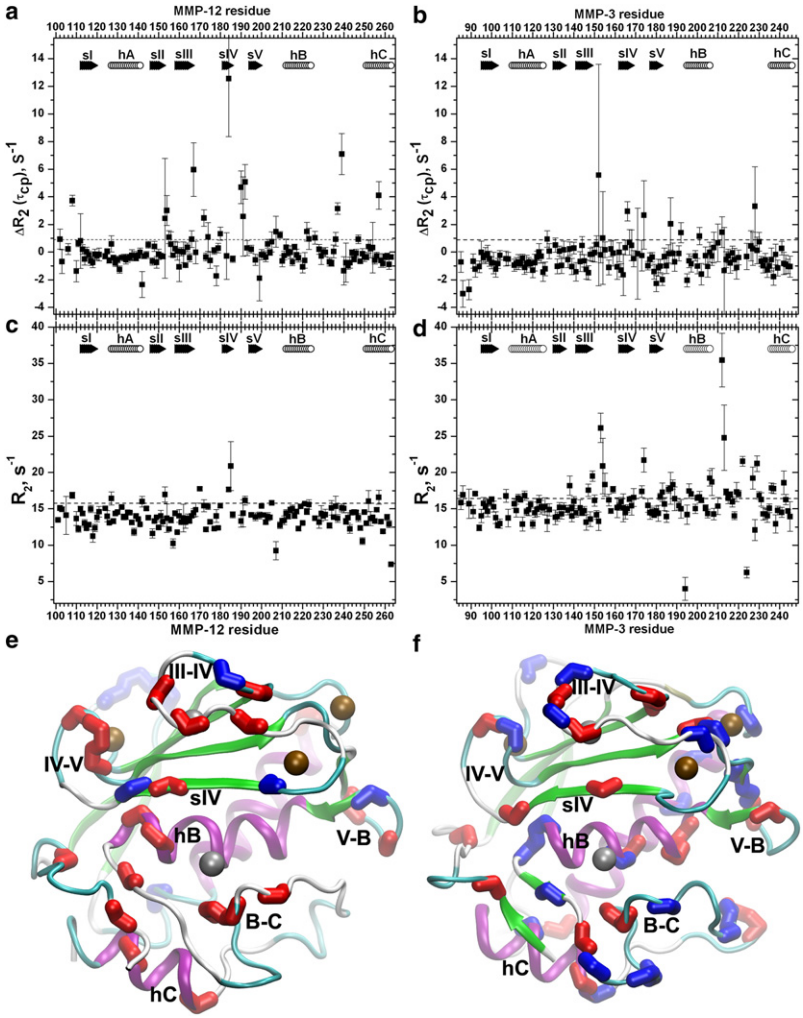

FIGURE 2 ^{15}N NMR line broadening evidences of millisecond fluctuations of MMP-12(E219A) (*left panels*) and MMP-3 catalytic domain (*right panels*) at 26°C and 61 MHz. (*a* and *b*) Relaxation-compensated TROSY-CPMG measurements of $\Delta R_2 = R_2(11\text{ ms}) - R_2(1.7\text{ ms})$ are plotted, where 11 and 1.67 ms are the spacings between π-pulses of the CPMG trains. (*c* and *d*) Spin-spin relaxation rate constant R_2 was measured using an HSQC-based sequence with 1.2 ms between π-pulses (26). (*Dashed lines*) Thresholds above which the excess line broadening is considered significant. The thresholds are drawn 2 s^{-1} above the mean R_2 after fine filtering-out of residues with internal motions (Table S2). Secondary structure is marked as in Fig. 1. (*e* and *f*) The structures of MMP-12(E219A) and MMP-3 catalytic domain, respectively, are depicted with red/lighter shading of bonds of residues with exchange broadening at 61 MHz, reproducing that at 81 MHz (Fig. 1). Blue/darker shading indicates bonds supplementary to 81-MHz data that did not quantify the broadening.

II–III loop, sIII, S-shaped III–IV loop, and hC of MMP-3 catalytic domain (Fig. 2, *b*, *d*, and *f*). The apparent exchange broadening of at least 84 residues of MMP-3 catalytic domain (at 81 and/or 61 MHz) suggests that they sample conformational substates.

Fast fluctuations

^{15}N R_1 at 51 MHz exceeding 2.1 s^{-1} serves as evidence for internal motions with apparent time constant $\tau_e > 1.1$ ns (35). Both MMPs display ^{15}N R_1 values at 51 MHz that are elevated above this threshold in their III–IV, IV–V, V-B, and B-C loops (Fig. S2, *a* and *b*). Some elevation of the ^{15}N R_1 values at 61 MHz (Fig. S2, *a* and *b*) may also corroborate motions of amide bonds in the low nanosecond regime in these four loops.

Steady-state $\{^1H\}^{15}N$ NOE values have median values of 0.76 and 0.75 for MMP-12(E219A) and MMP-3 catalytic domain, respectively (Fig. S2, *c* and *d*). More residues of MMP-3 catalytic domain have $\{^1H\}^{15}N$ NOEs below 0.7, suggesting that those positions are enhanced in subnanosecond fluctuations. The lower NOE values suggest more fast fluctuations in hA, sIV, IV–V loop, sV, V-B loop, hB, B-C loop, and hC of MMP-3 catalytic domain that may distinguish it from MMP-12(E219) (Fig. S2 *d*). Other segments of higher mobility in the II–III loop, III–IV loop, and S1′ specificity segment of the B-C loop of MMP-12(E219A) distinguish it (Fig. S2 *c*).

Hydrodynamics

An accurate model of rotational diffusion is needed for us to assess the contributions of internal motions to NMR relaxation in model-free calculations. Initial coarse filtering-out of mobile residues (29) leaves 99 residues of MMP-3 catalytic domain and 96 residues of MMP-12(E219A). Their mean ^{15}N NMR relaxation parameters are listed in Table S2 in the Supporting Material. Subsequent fine filtering removes residues with other evidences motions (30), leaving 37 residues of MMP-3 catalytic domain and 43 residues of MMP-12(E219A) that would be considered rigid enough for their ^{15}N relaxation to represent overall rotational diffusion.

This set of MMP-3 catalytic domain residues has mean values of ^{15}N R_1, R_2, and steady-state NOE at 26°C and 14.1 T, of 1.63 s^{-1}, 14.42 s^{-1}, and 0.77, respectively (Table S2). The set from MMP-12(E219A) has mean values of ^{15}N R_1, R_2 and NOE at 26°C and 14.1 T of 1.74 s^{-1}, 13.03 s^{-1}, and 0.76. The higher filtered R_2/R_1 ratio of MMP-3 catalytic domain suggests it may tumble slightly more slowly, with correlation time near 9.0 ns, relative to 8.7 ns for MMP-12(E219A) (Table S2). These correlation times are consistent with monodisperse character. Fitting of diffusion tensors to the rigid residues using TENSOR2 (31) suggests slight axial symmetry of rotational diffusion. The MMP-3 catalytic domain initially appears slightly more likely to behave as a prolate ellipsoid (Table S2). MMP-12(E219A) more clearly tumbles as an oblate ellipsoid with an apparent $D_{\|}/D_{\perp}$ of 0.88 (Table S2). Optimization of hydrodynamics parameters by model-free simulations revised $D_{\|}/D_{\perp}$ slightly to 0.89 for MMP-12(E219A) and more so to 0.70 (a prolate to oblate shift) for MMP-3 catalytic domain. These simulations left the rotational correlation time of MMP-12(E219A) at 8.66 ns and shifted that of MMP-3 catalytic domain down to 8.66 ns as well. These are less than reported for free MMP-1 catalytic domain at 9.7 ns (36) and inhibitor complexes of MMP-3 catalytic domain at 10.6–11.8 ns (23).

Model-free evidence of enhanced rigidity of some locations in MMP-12(E219A)

Spectral density functions of the model-free formalism were fitted to their ^{15}N relaxation shown in Fig. 2, *c* and *d*, and Fig. S2, *a–d*. The resulting generalized order parameter S^2 suggests amplitudes of amide bond reorientations that are faster than the correlation time of rotational protein diffusion. S^2 can range from 0 for full disorder to 1.0 for full restriction of bond reorientation on the fast timescale. R_{ex} reports excess line broadening attributable to dynamic equilibria such as conformational exchange (38). The value τ_e represents an apparent but qualitative time constant of internal bond reorientation (38). Counts of residues statistically requiring R_{ex} or τ_e are summarized in Table S3. Fitting with τ_e is required for 58 residues of MMP-12(E219A) and 54 of MMP-3 catalytic domain (Table S3 and Fig. S3). The S^2 values average 0.945 ± 0.045 and 0.928 ± 0.068 across MMP-12(E219A) and MMP-3 catalytic domain, respectively (Fig. 3, *a* and *b*). The secondary structure of each protease is similarly rigid. S^2 averages 0.95 over the helices and 0.96 across its β-sheet of MMP-12(E219A), compared to 0.94 over the helices and 0.92 across the β-sheet of MMP-3 catalytic domain.

Inspection of fitted S^2 and R_{ex} suggests that MMP-12(E219A) is more rigid than MMP-3 catalytic domain at some locations (Fig. 3). In particular, the locale just before and including hC is more rigid in MMP-12(E219A), with mean $\Delta S^2_{MMP12–MMP3} = 0.08$. Five of the seven residues rigidified on the subnanosecond scale in this segment of MMP-12(E219A) are conserved between the two proteases: Phe-248, Leu-250, Ser-251, Ile-255, and Gly-257 (Fig. 3 *e*). MMP-12(E219A) also exhibits greater rigidity of single residues in and near the β-sheet at sI, sIII, sIV, the IV–V loop, the V-B loop, and perhaps sV (Fig. 3, *a*, *b*, and *e*). Both decreased and increased rigidity may occur at a few positions within the III–IV and B-C loops (Fig. 3, *a*, *b*, and *e*). The E219A lesion in hB in MMP-12 seems to be enhanced in fast fluctuations relative to the wild-type Glu-203 counterpart of MMP-3 catalytic domain, i.e., its $\Delta S^2_{MMP12-MMP3} = -0.16$ (Fig. 3 *e*). This coincides with the very small cavity introduced by the smaller side chain (34).

The R_{ex} term is statistically warranted for model-free fitting of ^{15}N exchange broadening of 78 residues of MMP-3 catalytic domain and 54 residues of MMP-12(E219A) (Table S3). The statistics confirm most cases of broadening observed as elevated relaxation rates at 14.1 T. The statistics also suggest a need for small R_{ex} terms at some sites lacking clearly elevated relaxation rates, such as β-strand I of both proteases and in MMP-12 the I-A and A-II loops and much of hA and hB (Fig. 3, *c* and *d*). The R_{ex} terms of MMP-3 catalytic domain average larger at 4.8 s^{-1} than those of MMP-12(E219A) at 2.5 s^{-1}. Additional residues of MMP-3 catalytic domain needing R_{ex} terms appear in β-strands sI and sIII, helices hA and hC, and the III–IV, V-B and B-C loops (Fig. 3, *c*, *d*, and *f*).

MMP-3 catalytic domain is more stably protected from hydrogen exchange

We sought to compare the global and residue-specific stabilities of these two MMP catalytic domain, using NMR to measure the protection of their amide groups from hydrogen exchange (HX). In assessing how adequately MMP-12(E219A) may represent wild-type MMP-12 in such studies, we found them to be similarly sensitive to chemical denaturation within the uncertainties (Fig. S4).

HX behavior in the EX2 regime is an excellent means of measuring protein folding stability globally (39), subglobally, and locally (40). EX2 refers to the limit of HX where the closing of the hydrogen bond is much faster than the exchange step ($k_{cl} >> k_{rc}$), making the rate-limiting step the intrinsic rate of HX from the random coil state, k_{rc} (41). Consequently, the Gibbs free energy of protection of amide protons from HX in the EX2 regime can be calculated from measured rate constants of the exchange, k_{ex}, using Eq. 2.

EX2 hydrogen exchange behavior

After plunging each lyophilized MMP into D_2O, the ensuing HDX revealed that deuterons replace several amide protons of MMP-3 catalytic domain >10-fold more slowly than the slowest case in MMP-12(E219A) (Fig. S5, *a* and *b*). We investigated the HX regime by plotting measured k_{ex} against k_{rc} (42) and clustering them into tiers of similar

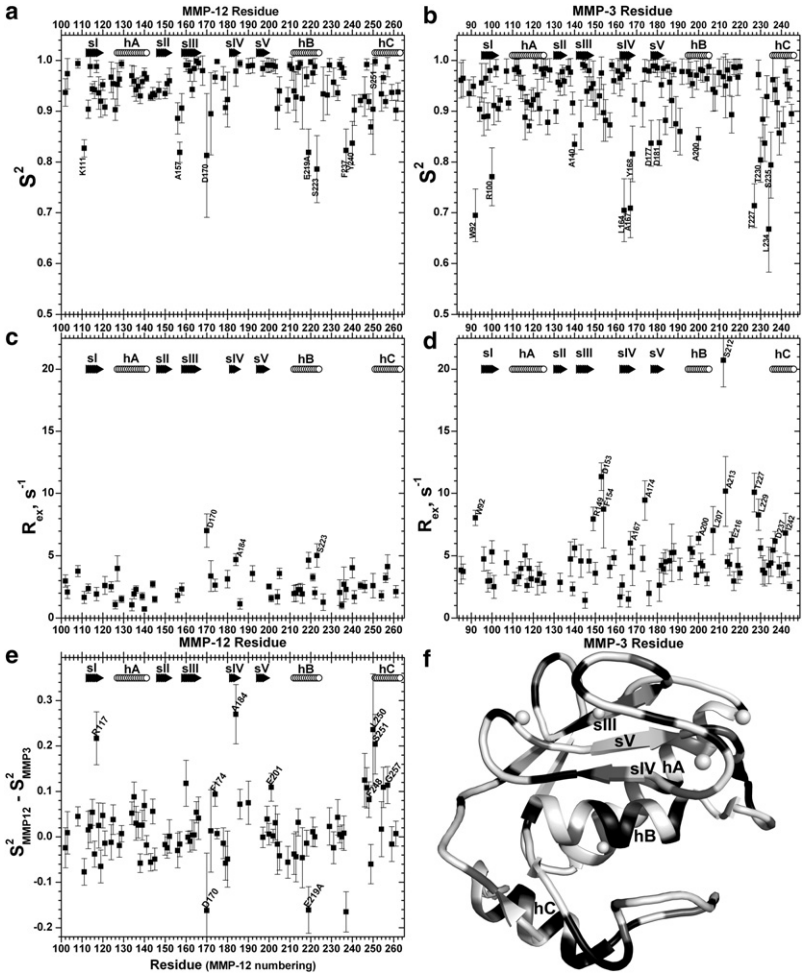

FIGURE 3 Model-free parameters fitted to ^{15}N relaxation (26°C) of MMP-12(E219A) (*panels* at *left*) and MMP-3 catalytic domain (*panels* at *right*), i.e., generalized order parameters S^2 (*a* and *b*) and line broadening term R_{ex} (*c* and *d*). (*e*) Differences in S^2 of MMP-12 (E219A) from the equivalent position in MMP-3 catalytic domain are plotted. Secondary structure is marked as in Fig. 1. (*f*) Solid representation indicates MMP-3 residues (PDB entry 1cqr) with $R_{ex} > 4\ s^{-1}$ and medium shading represents those with R_{ex} from 1 to 4 s^{-1}.

apparent stability to HDX (Fig. S5, *a* and *b*). The EX2 regime exhibits a theoretical slope of one and the EX1 regime a theoretical slope of zero in log-log plots of k_{ex} versus k_{rc} (42). The slopes of the tiers are much closer to one than zero for both MMP catalytic domain, even for the faster exchanging residues (Fig. S5, *a* and *b*). Thus, both MMP constructs appear to have $k_{cl} >> k_{rc}$ of 1000–1400 min^{-1} (Fig. S5, *a* and *b*), satisfying the EX2 limit and justifying the use of Eq. 2.

Stabilities

In MMP-12(E219A), at least 55 residues were protected from HDX. The bulk of them have an apparent $\Delta G_{HX,app}$ of 5.5–7.4 kcal/mol (Fig. 4 *a*). Several residues display higher apparent $\Delta G_{HX,app}$ in the range of 7.6–9.8 kcal, particularly in hA and hB, but also in sI and near the N-terminus of hC (Fig. 4 *a*). Averaging the three highest stabilities provides an initial estimate of global stability ΔG_{HX} (39) of 9.27 kcal/mol. Correction of ΔG_{HX} for proline *cis-trans* isomerization was shown to agree with traditional measurements of folding stability to within 1 kcal/mol (39). This uses the following expression and tabulated equilibrium constants for *cis-trans* proline isomerization K_{Pro} (39):

$$\Delta G_U = \Delta G^*_{HX} = \Delta G_{HX} - \sum(RT\ln(1 + K_{Pro})). \quad (3)$$

Crystal and solution structures of MMP-12 without inhibitor (PDB codes 2oxu and 2poj) show that its six prolines are in the *trans* conformation. The correction of 0.51 kcal/mol results in the estimate of folding stability of $\Delta G_{HX}* = 8.76$ kcal/mol for MMP-12(E219A) at 26°C.

More residues of MMP-3 catalytic domain, i.e., 79 residues, were protected from HDX. The bulk of its protected residues have $\Delta G_{HX,app}$ that ranges from 6.6 to 10.1 kcal/mol (Fig. 4 *b*). More stably protected amide groups are observed in sI, hA, sIII, sIV, sV, the C-terminal end of hB, and a few loops, with $\Delta G_{HX,app}$ ranging from 10.8 to 12.7 kcal/mol. Averaging the three highest $\Delta G_{HX,app}$ values among these provides an initial estimate of global stability (39) of 12.57 kcal/mol. The 11 prolines of the free state structure (PDB code 1cqr) are *trans*, leading to a correction for *cis-trans* isomerization of 1.06 kcal/mol. Thus, the folding stability $\Delta G_{HX}*$ of MMP-3 catalytic domain appears to be 11.52 kcal/mol, which is ~2.8 kcal/mol greater than MMP-12(E219A). All five

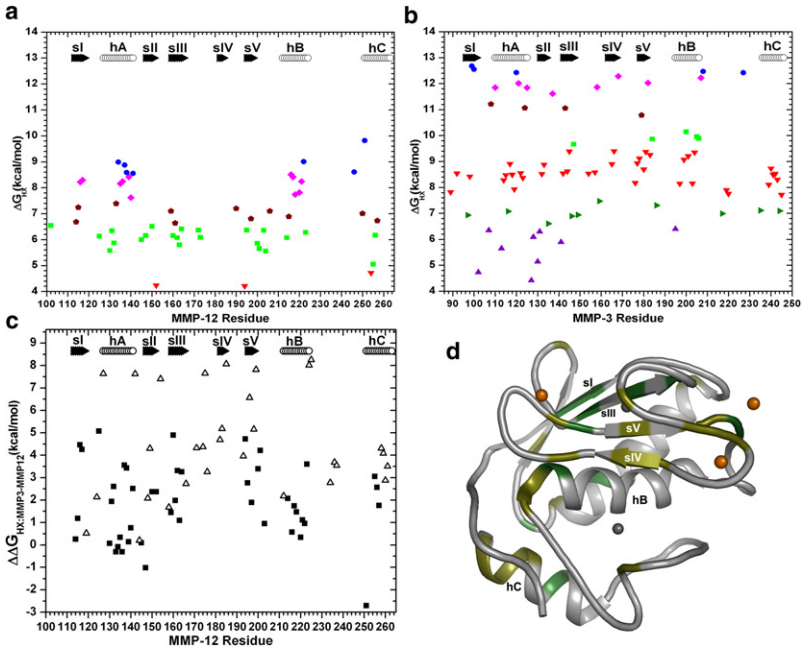

FIGURE 4 Comparison of apparent stabilities, ΔG_{HX}, of amide HDX of (*a*) MMP-12(E219A) and (*b*) MMP-3 catalytic domain. (*c*) Comparison of the ΔG_{HX} values of aligned residues in MMP-3 and -12. (*Open triangles*) Amide groups that are well protected from HDX in MMP-3 catalytic domain but for which $\Delta G_{HX,MMP12}$ could not be measured. These also represent a lower limit on $\Delta G_{HX,MMP3}$–$\Delta G_{HX,MMP12}$ that assumes an upper limit on $\Delta G_{HX,MMP12}$ of 4.2 kcal/mol, the smallest $\Delta G_{HX,MMP12}$ observed. (*d*) Locations where $\Delta G_{HX,MMP3}$–$\Delta G_{HX,MMP12}$ locally exceeds the global stability difference of 2.8 kcal/mol are shaded green/darker for residues with elevated black squares in *C* and olive/lighter for the open triangles elevated in *C*.

β-strands and all three helices of MMP-3 catalytic domain have amide groups that appear to be stabilized locally more than the 2.8 kcal/mol increase in overall folding stability relative to MMP-12(E219A) (Fig. 4, *b* and *c*). The largest of these localized increases in stability of >5 kcal/mol map to the sites in MMP-3 catalytic domain that lack measurable HDX protection of the equivalent positions in MMP-12(E219A) (*open triangles* in Fig. 4 *c*). The more stabilized locales of MMP-3 catalytic domain appear to be biggest across the β-sheet, but appear in the helices as well (Fig. 4, *c* and *d*).

DISCUSSION

More active MMP-12 versus more stable MMP-3

The greater activity of MMP-12 compared to MMP-3 catalytic domain is pronounced for substrates from protease-resistant elastin and collagens IV and V (Table 1). Structural descriptions of these homologs have not accounted for their differences in activity. Several residues of MMP-12 have recently been implicated in its specificity for fibrillar substrates (M. O. Palmier, Y. G. Fulcher, and S. R. Van Doren, unpublished). Substitutions of those MMP-12 residues modify its K_m for the elastin-derived substrate. However, the advantage of MMP-12 over MMP-3 is instead in k_{cat} (M. O. Palmier, Y. G. Fulcher, and S. R. Van Doren, unpublished). Biophysical properties may be important in accounting for MMP-12 advantages in k_{cat}. Higher rigidity and lower stability of MMP-12(E219A) have emerged to distinguish it from MMP-3 catalytic domain.

Structural facets of stabilities by HX

Transient openings of hydrogen bonds controlling apparent ΔG_{HX} can arise from rare global unfolding events related to global folding stability, as well as subglobal opening events and frequent, localized structural fluctuations (40). In MMP-12(E219A), the regions displaying high ΔG_{HX} approaching the global stability are confined to the helices and sI (Fig. 4 *a*). In MMP-3 catalytic domain, residues with high ΔG_{HX} approaching the global stability are distributed throughout the β-sheet region, hA, and hB (Fig. 4 *b*). Consequently, although the global stability of MMP-3 catalytic domain appears to be 2.8 kcal/mol greater than MMP-12(E219A), the β-sheet of MMP-3 catalytic domain has sites with $\Delta G_{HX,app}$ measured to be 4–5 kcal/mol higher than in MMP-12(E219A) (Fig. 4, *c* and *d*). Moreover, eight amide groups of MMP-3 catalytic domain would seem to have $\Delta G_{HX,app} > 7$ kcal/mol larger than their counterparts in MMP-12(E219A) with HDX too rapid to quantify (Fig. 4, *c* and *d*). This might be explained if the β-sheet of MMP-12(E219A) undergoes subglobal structural fluctuations that open its H-bonds and mask underlying smaller differences from MMP-3 catalytic domain in rare global opening events (with $\Delta\Delta G = 2.8$ kcal/mol).

Why is MMP-3 more stable than MMP-12?

Greater entropic stabilization is likely in MMP-3 catalytic domain. An exposed residue replaced by proline or an exposed glycine replaced by alanine typically stabilizes a protein by decreasing the configurational entropy of unfolding (44,45). Proline substitutions at exposed positions with dihedral angle ϕ near $-60°$, especially in β-turns and the N-cap position of helices, have consistently been stabilizing (46,47). Proline introduced to exposed turns at position $i+1$ in type I and i and $i+1$ in type II, stabilized several proteins in >90% of cases by an average of 0.7 kcal/mol (47). MMP-3 may also be stabilized by its substitutions of

proline at three such exposed sites: the N-cap of hA (Asn-126 in MMP-12), a turn in the III–IV loop (Ala-173 in MMP-12), and a type II′ turn of the IV–V loop (Ser-189 in MMP-12). Glycine substitutions decrease folding stability by stabilizing the unfolded state with greater configurational entropy (48). Inasmuch as MMP-12 possesses seven more glycines (Gly-106, -166, -179, -186, -192, -209, and -227) than the MMP-3 catalytic domain, MMP-12 should have a greater configurational entropy when unfolded and a lower folding stability as a result. The more extensive millisecond motions of MMP-3 catalytic domain around the active site lend enhanced configurational entropy that might stabilize its folded state relative to MMP-12.

Enzymes trading stability for function

Increased stability with loss of activity from point mutations of catalytically important residues was observed in the active sites of the enzymes staphylococcal nuclease, citrate synthase, barnase, T4 lysozyme, a β-lactamase, an enolase, and thermolysin, as reviewed by Shoichet et al. (2) and Beadle and Shoichet (3). These authors also noted tradeoffs of stability for affinity of mutant barstar for barnase and mutant λ Cro for DNA. Shoichet et al. (2) and Beadle and Shoichet (3) have articulated these cases into a general hypothesis of a balance between functional activity and destabilization of an active site. The destabilization is necessitated by the loss of stabilizing packing interactions within a protein needed to poise the active site to bind substrate and stabilize the transition state. Accumulating six stabilizing point mutations provided much less stabilization (3.7 kcal/mol) than summing the stabilization from each individual mutation (49). This parallels MMP-3 catalytic domain being 2.8 kcal/mol stabilized relative to MMP-12(E219A) despite 40% of their sequences differing.

The point mutations of the stability-function studies above were chosen to relieve strain at the active sites (3). Perhaps the greater rigidity and lower stability of MMP-12 are accompanied by greater strain at its active site, to support greater proteolytic activity than evidenced by the more relaxed and stable MMP-3 catalytic domain. The lesser folding stability and higher activity of MMP-12 could account for its rapid autolysis. Perhaps this foreshortens its lifetime of proteolytic attack upon sites of inflammation where it has been secreted by macrophages.

Comparison of flexibility

MMP-12 is the more rigid enzyme and MMP-3 the more flexible, with twofold as many residues with evidence of motion on the microsecond-to-millisecond timescale. These are concentrated around the active site region (Figs. 1 and 2). MMP-3 catalytic domain also has some subtly greater flexibility on the picosecond-to-nanosecond scale near the beginning of hC and isolated sites in β-strands I, III, IV, and V, loops flanking sIV and sV, and hA (Fig. 3 *e* and Fig. S2, *c* and *d*).

Comparison of MMP-3 catalytic domain, free and bound to inhibitors, suggests slow motions to be intrinsic to it. The extensive line broadening of MMP-3 catalytic domain implies that its greater flexibility extends to hundreds of microseconds to milliseconds (Fig. 1 and Fig. 2, *c* and *d*). Line broadening was also widespread but partly quenched in inhibitor complexes of MMP-3 catalytic domain, where R_{ex} terms $<2.8\ s^{-1}$ were needed for approximately half of residues (23). The majority of the residues in the free state require model-free R_{ex} terms averaging $4.8\ s^{-1}$ (Fig. 3 *d*). The broadening is exaggerated to a median $>9\ s^{-1}$ in the analysis of Fig. 1, *b* and *d*. These results indicate that sampling of conformational substates within milliseconds is characteristic of the region around the active site of MMP-3 catalytic domain (Fig. 1, *f* and *h*).

Less but significant exchange broadening maps were found around the active site of MMP-12(E219A) as well (Fig. 1). Based on greater depth of hB in its free state in solution and ^{1}H line broadening and splitting throughout hB, a slow conformational equilibrium affecting the depth of hB was hypothesized (34). The ^{15}N line broadening now evident around the active site and hB of both MMP-12 and MMP-3 (Figs. 1 and 2, and Fig. 3, *c* and *d*) could be consistent with the possibility of slow breathing fluctuations that might allow small changes in depth of hB or fraying of its termini.

Parallels with MMP-1 and -13

The comparison of MMP-12 with MMP-3 may be paralleled by how MMP-13 (collagenase 3) compares with MMP-1 (collagenase 1). MMP-13 tends to be more active than MMP-1 (50,51). Though MMP-13 and -1 share average S^2 of 0.88 overall, MMP-13 is in some respects more rigid than MMP-1. In the key S1′ specificity loop, MMP-1 has higher-amplitude subnanosecond fluctuations (low S^2) than MMP-13 (22), greater line broadening evidence of millisecond fluctuations, and splitting of peaks in hB (36). The most obvious NMR line broadening of MMP-13 (22) coincides with that of MMP-12 and -3 at the N-terminus, C-termini of hA and hB, sIV, and in hC, particularly around the periphery of the active site. Thus, sampling of conformational substates around the active sites may be characteristic of all four MMPs.

Possible roles for conformational substates

The slow mobility encompassing the active sites of MMP-3 and -12 suggests an intrinsic plasticity that could facilitate their recognition and the hydrolysis of diverse protein substrates. The native-state ensemble of conformations of MMP-12 may be better poised than MMP-3 to populate catalytically competent substates. These substates should stabilize the transition state to accelerate proteolytic turnover, manifest as k_{cat}. The apparently more extensive sampling of conformational substates of the active sites of MMP-3 (Fig. 1) and MMP-1 (36) coincides with their lower activities (Table 1) (50,51). Perhaps the more readily populated alternative conformers of the active site of MMP-3 may be

analogous to binding-incompetent substates, which were recently described in engineered adenylate kinase that had line broadening (more severe than in MMP-3) and lower affinity (53). If a greater population of alternative conformers or the MMP-3 active site are functionally incompetent, this might account for the lower catalytic turnover k_{cat} (M. O. Palmier, Y. G. Fulcher, and S. R. Van Doren, unpublished), lower catalytic efficiency k_{cat}/K_m (Table 1), and apparently less avid inhibition by small MMP inhibitors.

The differences in flexibility of MMP-3 and -12 are not restricted to the active site region (Fig. 1, *e–h*, and Fig. 3). Cooper and Dryden (54) argued, by using statistical thermodynamics, that cooperativity and long-range communication between separated sites can be mediated by diverse changes in frequency and amplitude of motions induced by binding, in the absence of conformational change. This hypothesis of allostery, mediated by changes of entropy without conformational change, may engage proximal and distal dynamics in regulating function not only in adenylate kinase (53), calmodulin (55), and MMPs, but in many proteins and enzymes (1).

SUPPORTING MATERIAL

Five figures and three tables are available at http://www.biophysj.org/biophysj/supplemental/S0006-3495(10)00433-9.

We thank G. B. Fields and J. Lauer for the triple-helical peptide substrate.

This work was funded by National Institutes of Health (NIH) grant No. GM572389 and American Heart Association grants No. 0455885Z and No. 0855714G. Nuclear magnetic resonance spectrometers were purchased with funding from the University of Missouri and NIH grant No. RR022341 toward the Avance 800 MHz system (Bruker AXS, Madison, WI), and the University of Missouri and National Science Foundation grant No. DBI-0070359 and NIH grant No. GM57289 toward the Innova 600 MHz system (Varian, Salt Lake City, UT). Data for Fig. 1, *a* and *c*, were collected using the Inova 800 MHz system (Varian) of the Environmental Molecular Sciences Laboratory, a U.S. Department of Energy Office of Biological and Environmental Research national user facility located at the Pacific Northwest National Laboratory. Data for Fig. S3, *a* and *b*, were collected with a DMX-500 system (Bruker AXS) at The National Magnetic Resonance Facility at Madison, supported by NIH grants No. P41RR02301and No. P41GM66326. T.S.B. was supported by NIH training grant No. GM008396.

REFERENCES

1. Boehr, D. D., H. J. Dyson, and P. E. Wright. 2006. An NMR perspective on enzyme dynamics. *Chem. Rev.* 106:3055–3079.
2. Shoichet, B. K., W. A. Baase, …, B. W. Matthews. 1995. A relationship between protein stability and protein function. *Proc. Natl. Acad. Sci. USA.* 92:452–456.
3. Beadle, B. M., and B. K. Shoichet. 2002. Structural bases of stability-function tradeoffs in enzymes. *J. Mol. Biol.* 321:285–296.
4. Shapiro, S. D., D. K. Kobayashi, and T. J. Ley. 1993. Cloning and characterization of a unique elastolytic metalloproteinase produced by human alveolar macrophages. *J. Biol. Chem.* 268:23824–23829.
5. Dean, R. A., J. H. Cox, …, C. M. Overall. 2008. Macrophage-specific metalloelastase (MMP-12) truncates and inactivates ELR + CXC chemokines and generates CCL2, -7, -8, and -13 antagonists: potential role of the macrophage in terminating polymorphonuclear leukocyte influx. *Blood.* 112:3455–3464.
6. Antonicelli, F., G. Bellon, …, W. Hornebeck. 2007. Elastin-elastases and inflamm-aging. *Curr. Top. Dev. Biol.* 79:99–155.
7. Houghton, A. M., P. A. Quintero, …, S. D. Shapiro. 2006. Elastin fragments drive disease progression in a murine model of emphysema. *J. Clin. Invest.* 116:753–759.
8. Johnson, J. L., S. J. George, …, C. L. Jackson. 2005. Divergent effects of matrix metalloproteinases 3, 7, 9, and 12 on atherosclerotic plaque stability in mouse brachiocephalic arteries. *Proc. Natl. Acad. Sci. USA.* 102:15575–15580.
9. Curci, J. A., S. Liao, …, R. W. Thompson. 1998. Expression and localization of macrophage elastase (matrix metalloproteinase-12) in abdominal aortic aneurysms. *J. Clin. Invest.* 102:1900–1910.
10. Lauer-Fields, J. L., T. Sritharan, …, G. B. Fields. 2003. Selective hydrolysis of triple-helical substrates by matrix metalloproteinase-2 and -9. *J. Biol. Chem.* 278:18140–18145.
11. Fu, J. Y., A. Lyga, …, D. Chen. 2001. Cloning, expression, purification, and characterization of rat MMP-12. *Protein Expr. Purif.* 21:268–274.
12. Bhaskaran, R., M. O. Palmier, …, S. R. Van Doren. 2008. MMP-12 catalytic domain recognizes triple helical peptide models of collagen V with exosites and high activity. *J. Biol. Chem.* 283:21779–21788.
13. Gronski, Jr., T. J., R. L. Martin, …, S. D. Shapiro. 1997. Hydrolysis of a broad spectrum of extracellular matrix proteins by human macrophage elastase. *J. Biol. Chem.* 272:12189–12194.
14. Hembry, R. M., M. R. Bagga, …, D. L. Hamblen. 1995. Immunolocalization studies on six matrix metalloproteinases and their inhibitors, TIMP-1 and TIMP-2, in synovia from patients with osteo- and rheumatoid arthritis. *Ann. Rheum. Dis.* 54:25–32.
15. Gurney, K. J., E. Y. Estrada, and G. A. Rosenberg. 2006. Blood-brain barrier disruption by stromelysin-1 facilitates neutrophil infiltration in neuroinflammation. *Neurobiol. Dis.* 23:87–96.
16. Lang, R., A. Kocourek, …, K. Maskos. 2001. Substrate specificity determinants of human macrophage elastase (MMP-12) based on the 1.1 Å crystal structure. *J. Mol. Biol.* 312:731–742.
17. Nar, H., K. Werle, …, B. Jung. 2001. Crystal structure of human macrophage elastase (MMP-12) in complex with a hydroxamic acid inhibitor. *J. Mol. Biol.* 312:743–751.
18. Shipley, J. M., G. A. Doyle, …, R. M. Senior. 1996. The structural basis for the elastolytic activity of the 92-kDa and 72-kDa gelatinases. Role of the fibronectin type II-like repeats. *J. Biol. Chem.* 271:4335–4341.
19. Collier, I. E., P. A. Krasnov, …, G. I. Goldberg. 1992. Alanine scanning mutagenesis and functional analysis of the fibronectin-like collagen-binding domain from human 92-kDa type IV collagenase. *J. Biol. Chem.* 267:6776–6781.
20. Tam, E. M., T. R. Moore, …, C. M. Overall. 2004. Characterization of the distinct collagen binding, helicase and cleavage mechanisms of matrix metalloproteinase 2 and 14 (gelatinase A and MT1-MMP): the differential roles of the MMP hemopexin *c* domains and the MMP-2 fibronectin type II modules in collagen triple helicase activities. *J. Biol. Chem.* 279:43336–43344.
21. Bertini, I., V. Calderone, …, P. Turano. 2005. Conformational variability of matrix metalloproteinases: beyond a single 3D structure. *Proc. Natl. Acad. Sci. USA.* 102:5334–5339.
22. Moy, F. J., P. K. Chanda, …, R. Powers. 2000. High-resolution solution structure of the catalytic fragment of human collagenase-3 (MMP-13) complexed with a hydroxamic acid inhibitor. *J. Mol. Biol.* 302:671–689.
23. Yuan, P., V. P. Marshall, …, B. J. Stockman. 1999. Dynamics of stromelysin/inhibitor interactions studied by ^{15}N NMR relaxation measurements: comparison of ligand binding to the S1-S3 and S′1-S′3 subsites. *J. Biomol. NMR.* 15:55–64.
24. Wang, C., M. Rance, and A. G. Palmer, 3rd. 2003. Mapping chemical exchange in proteins with MW > 50 kD. *J. Am. Chem. Soc.* 125:8968–8969.

25. Liu, Y., and J. H. Prestegard. 2008. Direct measurement of dipole-dipole/CSA cross-correlated relaxation by a constant-time experiment. *J. Magn. Reson.* 193:23–31.

26. Farrow, N. A., R. Muhandiram, …, L. E. Kay. 1994. Backbone dynamics of a free and phosphopeptide-complexed Src homology 2 domain studied by ^{15}N NMR relaxation. *Biochemistry.* 33:5984–6003.

27. Loria, J. P., M. Rance, and A. G. Palmer, 3rd. 1999. A TROSY CPMG sequence for characterizing chemical exchange in large proteins. *J. Biomol. NMR.* 15:151–155.

28. Yip, G. N. B., and E. R. P. Zuiderweg. 2005. Improvement of duty-cycle heating compensation in NMR spin relaxation experiments. *J. Magn. Reson.* 176:171–178.

29. Pawley, N. H., C. Wang, …, L. K. Nicholson. 2001. An improved method for distinguishing between anisotropic tumbling and chemical exchange in analysis of ^{15}N relaxation parameters. *J. Biomol. NMR.* 20:149–165.

30. Ding, Z., G.-I. Lee, …, S. R. Van Doren. 2005. PhosphoThr peptide binding globally rigidifies much of the FHA domain from *Arabidopsis* receptor kinase-associated protein phosphatase. *Biochemistry.* 44:10119–10134.

31. Dosset, P., J. C. Hus, …, D. Marion. 2000. Efficient analysis of macromolecular rotational diffusion from heteronuclear relaxation data. *J. Biomol. NMR.* 16:23–28.

32. d'Auvergne, E. J., and P. R. Gooley. 2003. The use of model selection in the model-free analysis of protein dynamics. *J. Biomol. NMR.* 25: 25–39.

33. Bai, Y., J. J. Englander, …, S. W. Englander. 1995. Thermodynamic parameters from hydrogen exchange measurements. *Methods Enzymol.* 259:344–356.

34. Bhaskaran, R., M. O. Palmier, …, S. R. Van Doren. 2007. Solution structure of inhibitor-free human metalloelastase (MMP-12) indicates an internal conformational adjustment. *J. Mol. Biol.* 374:1333–1344.

35. Jin, D., M. Andrec, …, R. M. Levy. 1998. Propagation of experimental uncertainties using the Lipari-Szabo model-free analysis of protein dynamics. *J. Biomol. NMR.* 12:471–492.

36. Moy, F. J., M. R. Pisano, …, R. Powers. 1997. Assignments, secondary structure and dynamics of the inhibitor-free catalytic fragment of human fibroblast collagenase. *J. Biomol. NMR.* 10:9–19.

37. Reference deleted in proof.

38. Jarymowycz, V. A., and M. J. Stone. 2006. Fast time scale dynamics of protein backbones: NMR relaxation methods, applications, and functional consequences. *Chem. Rev.* 106:1624–1671.

39. Huyghues-Despointes, B. M., J. M. Scholtz, and C. N. Pace. 1999. Protein conformational stabilities can be determined from hydrogen exchange rates. *Nat. Struct. Biol.* 6:910–912.

40. Bai, Y., T. R. Sosnick, …, S. W. Englander. 1995. Protein folding intermediates: native-state hydrogen exchange. *Science.* 269:192–197.

41. Clarke, J., and L. S. Itzhaki. 1998. Hydrogen exchange and protein folding. *Curr. Opin. Struct. Biol.* 8:112–118.

42. Yan, S., S. D. Kennedy, and S. Koide. 2002. Thermodynamic and kinetic exploration of the energy landscape of *Borrelia burgdorferi* OspA by native-state hydrogen exchange. *J. Mol. Biol.* 323:363–375.

43. Reference deleted in proof.

44. Matthews, B. W., H. Nicholson, and W. J. Becktel. 1987. Enhanced protein thermostability from site-directed mutations that decrease the entropy of unfolding. *Proc. Natl. Acad. Sci. USA.* 84:6663–6667.

45. Street, T. O., C. M. Bradley, and D. Barrick. 2005. An improved experimental system for determining small folding entropy changes resulting from proline to alanine substitutions. *Protein Sci.* 14:2429–2435.

46. Watanabe, K., T. Masuda, …, Y. Suzuki. 1994. Multiple proline substitutions cumulatively thermostabilize *Bacillus cereus* ATCC7064 oligo-1,6-glucosidase. Irrefragable proof supporting the proline rule. *Eur. J. Biochem.* 226:277–283.

47. Fu, H., G. R. Grimsley, …, C. N. Pace. 2009. Increasing protein stability by improving β-turns. *Proteins.* 77:491–498.

48. D'Aquino, J. A., J. Gómez, …, E. Freire. 1996. The magnitude of the backbone conformational entropy change in protein folding. *Proteins.* 25:143–156.

49. Nagatani, R. A., A. Gonzalez, …, P. C. Babbitt. 2007. Stability for function trade-offs in the enolase superfamily ''catalytic module''. *Biochemistry.* 46:6688–6695.

50. Neumann, U., H. Kubota, …, D. Leppert. 2004. Characterization of Mca-Lys-Pro-Leu-Gly-Leu-Dpa-Ala-Arg-NH2, a fluorogenic substrate with increased specificity constants for collagenases and tumor necrosis factor converting enzyme. *Anal. Biochem.* 328:166–173.

51. Lauer-Fields, J. L., and G. B. Fields. 2002. Triple-helical peptide analysis of collagenolytic protease activity. *Biol. Chem.* 383:1095–1105.

52. Reference deleted in proof.

53. Schrank, T. P., D. W. Bolen, and V. J. Hilser. 2009. Rational modulation of conformational fluctuations in adenylate kinase reveals a local unfolding mechanism for allostery and functional adaptation in proteins. *Proc. Natl. Acad. Sci. USA.* 106:16984–16989.

54. Cooper, A., and D. T. Dryden. 1984. Allostery without conformational change. A plausible model. *Eur. Biophys. J.* 11:103–109.

55. Frederick, K. K., M. S. Marlow, …, A. J. Wand. 2007. Conformational entropy in molecular recognition by proteins. *Nature.* 448:325–329.

56. Palmier, M. O., and S. R. Van Doren. 2007. Rapid determination of enzyme kinetics from fluorescence: overcoming the inner filter effect. *Anal. Biochem.* 371:43–51.

57. Chen, L., T. J. Rydel, …, B. L. Barnett. 1999. Crystal structure of the stromelysin catalytic domain at 2.0 Å resolution: inhibitor-induced conformational changes. *J. Mol. Biol.* 293:545–557.